



# Low-cost scalable printing of carbon nanotube electrodes on elastomeric substrates: Towards the industrial production of EAP transducers



I. Burda<sup>a</sup>, C. Baechler<sup>a,\*</sup>, S. Gardin<sup>a</sup>, A. Verma<sup>b</sup>, G.P. Terrasi<sup>a</sup>, G. Kovacs<sup>a</sup>

<sup>a</sup> Empa, Swiss Federal Laboratories for Materials Testing and Research, Laboratory for Mechanical System Engineering, Überlandstrasse 129, 8600 Dübendorf, Switzerland

<sup>b</sup> Empa, Swiss Federal Laboratories for Materials Testing and Research, Laboratory for Functional Polymers, Überlandstrasse 129, 8600 Dübendorf, Switzerland

## ARTICLE INFO

### Article history:

Received 23 August 2017

Received in revised form 31 May 2018

Accepted 11 July 2018

### Keywords:

Stretchable electrodes

Gravure printing

Plasma treatment

Electro-mechanical characterization

## ABSTRACT

Dielectric elastomer transducers are promising devices for a growing field of applications. However, to be competitive with established electromechanical transducer technologies, low-cost and efficient fabrication process is needed. In particular, the electrode composition and deposition method seem to be the key elements in this context. In this paper, authors use gravure printing for the deposition of thin and compliant MWCNT electrodes on PDMS films. Gravure printing is a high through put deposition method which allows printing complex electrode patterns with high resolution and, therefore, is well suited for large scale production of dielectric elastomer transducers. Special attention was given to the adaptation of the MWCNT-based ink to the specific requirements of the gravure printing process in order to achieve stable and high quality printing. Furthermore, the effect of oxygen plasma treatment of the silicone substrate on the electro-mechanical behavior of electrode was investigated. In this context a comprehensive characterization of the electrodes behavior under uniaxial and biaxial strain was carried out. Two mechanisms that explain specific aspects of electro-mechanical behavior of electrodes are proposed.

© 2018 Elsevier B.V. All rights reserved.

## 1. Introduction

In recent years the development of stretchable transducers and sensors based on the deformation of elastomers has received significant interest [1]. Envisaged application of such novel compliant and damage resilient transducers are sensors [2,3], high-strain electroactive actuators [4,5], stretchable energy storage and conversion devices [6], or artificial muscles [7–9]. Silicone elastomers are appealing materials as elastomer dielectric for stretchable capacitors. They are lightweight, can be processed easily using a variety of methods, and are highly compliant. Besides that, silicone elastomers are available in a wide range of elastic moduli, generally possess low viscous properties leading to fast electromechanical response times, and can, as is the case for polydimethylsiloxane (PDMS), be optically transparent [10,11].

One of the main challenges, which stretchable transducers are confronted with, are requirements imposed to the electrodes: they

must encompass both flexibility and stretchability [12–14]. A substantial amount of research has been carried out on conductive polymer composites [15,16], metal electrodes [17–19], and materials based on carbon nanotubes and graphene [20–23]. In this paper we investigate gravure printing, an industrial fabrication method for the production of large-area high-resolution thin films, to print multiwall carbon nanotubes (MWCNT) electrodes on a PDMS film. MWCNTs possess high intrinsic conductivity and aspect ratio. This allows applying very thin electrodes in the range of a few tens of nanometers which exhibit the required conductivity and compliance. They can also be dispersed in a liquid medium in order to be deposited with conventional techniques developed for printed electronics. However, one of the main advantages of the MWCNTs is their relatively low price. This makes them a perfect material for large-scale production.

Gravure printing represents a perfect electrode deposition method, as it is compatible with roll to roll (R2R) production, allows large throughput (60 m<sup>2</sup>/s), high resolution (20 μm), lower materials consumption and faster process speeds (600 m/s) compared with other techniques, such as screen printing or inkjet printing [24–27]. Great emphasis will also be given to the effect of plasma

\* Corresponding author.

E-mail address: [Curdin.Baechler@empa.ch](mailto:Curdin.Baechler@empa.ch) (C. Baechler).

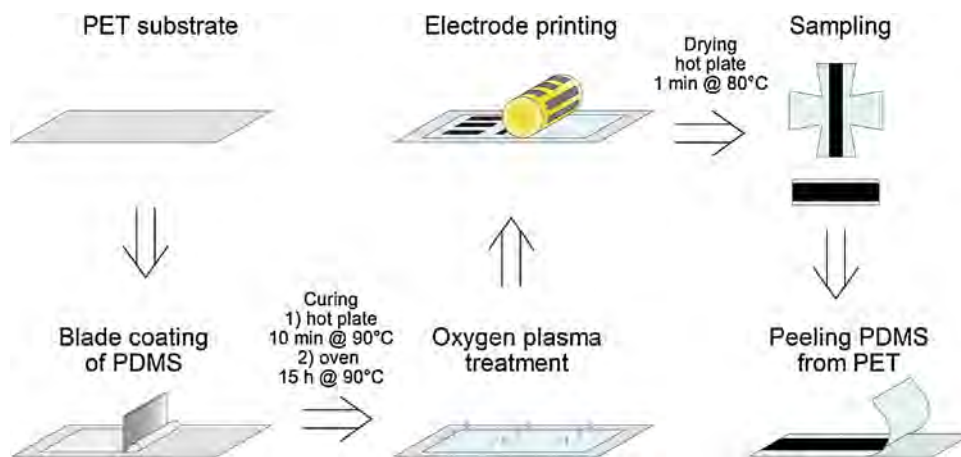


Fig. 1. Schematic illustration of PDMS film production, electrode deposition and sample preparation.

treatment on the final compliancy of the deposited electrode. We will analyze the impact of a brittle silica-like layer generated on the PDMS surface during plasma exposition on the electro-mechanical behavior of the electrode under uniaxial and biaxial straining.

## 2. Experimental methods

### 2.1. Ink preparation and characterization

The employed conductive ink is based on MWCNT (NANOCYL, grade NC7000™) with an average diameter and length of 9.5 nm and 1.5  $\mu\text{m}$  respectively. First a 4 wt% stock suspension was prepared by dispersing 2 g MWCNT into 46 ml of deionized water containing 2 g of an acrylic block copolymer dispersant (Efka PX4701). The MWCNT powder was added in steps of 0.4 g, and after each step the mixture was sonicated under stirring for 30 min using an ultrasonic processor (UP400S, Hielscher, 20% power setting) with a H14 sonotrode. In order to adapt the ink properties to gravure requirements, the MWCNT-suspension was modified by co-solvents. Propylene glycol n-propyl ether (PnP) was added to decrease the ink surface tension, and propylene glycol (PG) in order to increase its viscosity and drying time. Accordingly, a typical 1 wt% MWCNT ink was prepared by mixing 5 g stock solution with 1 g PnP and 14 g of PG. This mixture was again homogenized by sonication for 30 min A 5  $\mu\text{m}$  polypropylene syringe filter was used at the end to remove remaining large particles and agglomerates. The ink viscosity was measured at 20 °C by a strain controlled rheometer (Anton-Paar MCR 301) with a plate/plate geometry (25 mm diameter, 0.1 mm gap). A Drop Shape Analyzer (Krüss DSA30) was used to characterize the ink surface tension as well as the contact angle of the ink on the PDMS substrate. The reported values are the average of 5 measurements. The time between contact angle measurement and plasma treatment of the PDMS was 3 min.

### 2.2. Production of PDMS films with electrodes

The process of PDMS film production, electrode deposition and sample preparation is schematically illustrated in Fig. 1. Firstly, a 125  $\mu\text{m}$  thick Mylar A polyester (PET) substrates was manually cut to the size 230  $\times$  180 mm, which is somewhat bigger than the planned size of PDMS film. These PET substrates provide mechanical support for PDMS films and ease their handling during production and printing process. Afterwards, a custom made two compound silicone (EAP30, Wacker) was prepared by mixing 1:1 (by weight) component A and B with a static mixer. After degassing the mixture in a vacuum desiccator for 5 min., a 150  $\mu\text{m}$  thick film

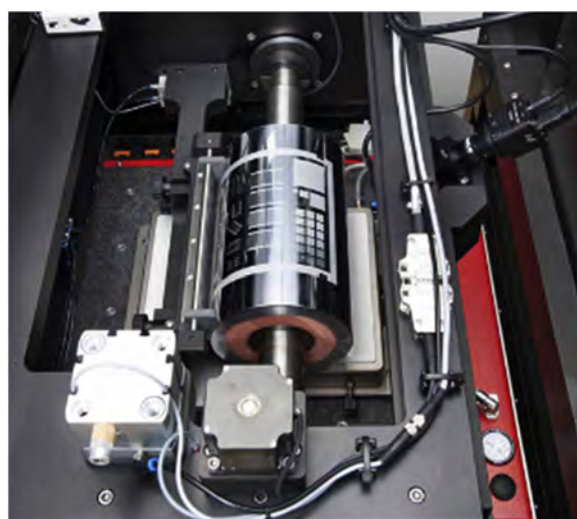


Fig. 2. Gravure printing module of a printing facility Challenger C600.

was blade coated on the PET substrate. The size of PDMS film was 210  $\times$  148 mm, which corresponds to the size of A5 paper. Such size was defined based on the dimensions of the vacuum chuck of the gravure printing facility.

The thickness of the PDMS film was chosen to be higher than is usually reported for EAP application. This was done in order to prevent extensive straining during removal of PDMS films from the PET substrates, which might damage both film and the deposited on it electrode. Moreover, the thicker PDMS films provided more convenient handling during characterization. The blade coated PDMS film was cured on a hot plate set at 90 °C for 10 min and then in an oven at 90 °C for about 15 h to ensure complete degree of cross-linking.

In order to provide sufficient wetting of PDMS film during the electrode printing a surface activation was carried out in a Plasma Chamber (Diener Atto) with 40 kHz / 100 W generator. The PDMS films were exposed to oxygen plasma (oxygen process pressure 0.5 mbar, generator power 75%). Different plasma treatment doses were achieved by varying the process time from 2 to 60 s while keeping all other parameters constant. The time between the end of the plasma treatment process and printing of the electrode never exceeded 3 min.

Deposition of the electrode was carried out using gravure printing module (Fig. 2) of a printing facility Challenger C600 (manufacturer nsm Schläfli AG). The printing process was performed in a clean room environment of Class 6. The ink for electrode deposition

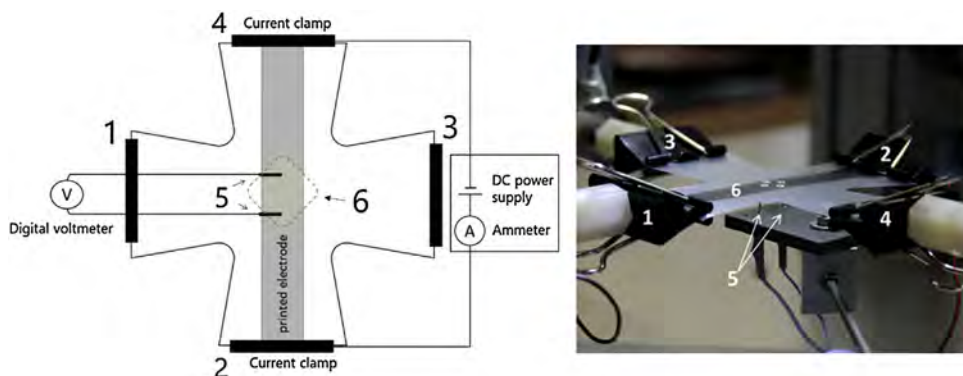


**Fig. 3.** Biaxial testing facility used for characterization of the electro-mechanical behavior of the electrodes. The cross-shaped sample is fixed in four clamps (1–4). Clamps 1 and 2 are also used to conduct direct current through the electrode. The potential drop over 1 cm distance was recorded by two voltage probes (5) within the region of homogenous strain state (6).

was prepared one day before printing. The printing machine allows to precisely adjust printing speed and the pressure between the gravure cylinder and the substrate by varying the height between the substrate and the gravure cylinder. The gravure cylinder used for this study has several rectangular shape engraved features with same cell densities, but different cell depth ( $8\ \mu\text{m}$ ,  $16\ \mu\text{m}$  and  $24\ \mu\text{m}$ ), allowing printing three different electrode thicknesses simultaneously on a single PDMS film. After printing the samples were dried on the hot plate at  $80\ ^\circ\text{C}$  for 1 min.

After the deposition of the electrode, the necessary samples were cut for electromechanical characterization. Prior to testing, the PDMS films were peeled from the PET substrate.

### 2.3. Surface characterization methods

In order to study topography and measure the thickness of the printed electrodes an AFM (Bruker ICON3) was used. The AFM was operated in PeakForce Tapping mode using ScanAsyst-Air cantilevers with nominal tip radius 2 nm. To measure the electrode thickness, line scans were performed across grooves which were made beforehand by peeling off a narrow strip of the deposited electrode using an adhesive tape. The thickness was obtained by determining the step height of a profile scan across the groove. The reported thickness is the average of 9 measured step heights across three different grooves.

### 2.4. Electro-mechanical characterization

The electro-mechanical characterization of the electrodes was done by performing periodical measurements of their electrical resistance upon biaxial straining (Fig. 3). The straining was performed using a biaxial testing facility (Zwick/Roell), which is equipped with four independently controllable actuators and four load cells with maximum capacity  $\pm 100\ \text{N}$ .

The samples for electro-mechanical characterization were cut in cross-shape. The shape and size of the sample enabled a sufficiently large homogeneous biaxial strain field [28], within which the measurements of electrical resistance were carried out.

The biaxial testing facility is equipped with video-extensometer that measures deformation and strain in multiple directions. A mixed force-displacement control mode was used for the straining. The clamped sample was stepwisely deformed by four actuators that were driven with constant displacement rate of 4 mm/min. During the deformation the load was continuously monitored and used to stop the actuators when all four load cells reached a certain value. After each straining step, the force was kept constant for 30 s and the electrical resistance was measured as described below.

The drop of load due to relaxation within the pause period was determined not to exceed 1% at maximum load. Prior to the electro-mechanical characterization, calibration tests were carried out to determine load-strain relation and the appropriate load values for the strains of interest. As the deviation of thickness of blade-coated PDMS layers was determined to be fairly small ( $150 \pm 15\ \mu\text{m}$ ), the load-strain relation was assumed to be the same for all samples.

Three nominal biaxial strain ranges (i.e. 0–4%, 0–8%, 0–12 %, achieved by corresponding loads of 0–0.8 N, 0–1.5 N and 0–2.2 N respectively) were applied to each sample in order to characterize their electro-mechanical response to increasing biaxial strain. For each strain range, up to two cycles were performed to investigate possible changes in the electromechanical behavior due to electrode damages induced from previous straining cycle.

Uniaxial straining was done in the same manner but only using one pair of actuators.

The measurements of electrical resistance were carried out according to a four-point probe technique, in which direct current ( $I = 20\ \mu\text{A}$ ) was conducted via the printed electrode and the potential drop was measured with a digital voltmeter (Brymen BM616). The pins for the potential drop measurements were applied to the region of the electrode, where the biaxial strain field is homogeneous.

## 3. Results and discussion

### 3.1. Ink development and characterization

Gravure printing poses some basic requirements regarding ink characteristics that must be fulfilled in order to achieve stable print results. The main properties, which control the ink transfer and printed layer quality are surface tension, viscosity and drying behavior. Surface tension plays an important role for the wetting of the substrate and for the leveling of the deposited liquid layer. Typical values for surface tension in gravure printing are in the range of 23–44 mN/m [29]. The initial MWCNT-water based ink (without any co-solvents) had a surface tension in the range of 46 mN/m which turned out to be too high for proper wetting even when the PDMS substrate was plasma treated.

This issue could be circumvented by the addition of 5 wt% PnP ( $25.4\ \text{mN/m}$ ) which reduced the surface tension to 34 mN/m. However, although this ink could be used for whole-surface printing, it was not suitable to print structured electrodes. Independent of print settings, there were always diffuse edges and ink spreading perpendicular to the printing direction (see Fig. 4a) The reason for it was found in the low viscosity of the ink ( $< 2\ \text{mPa}\cdot\text{s}$ ) which is significantly lower compared to standard inks for graph-

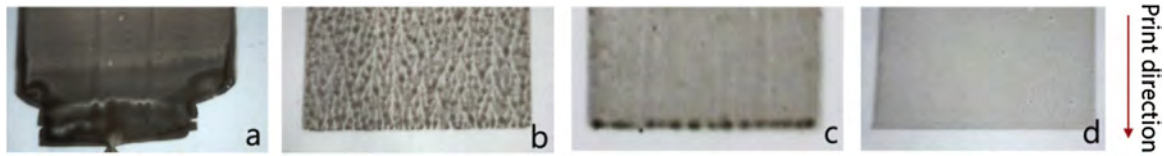


Fig. 4. Printing results of ink a–d showing the main ink development steps.

Table 1

Compositions (wt%) and viscosity (mPa·s) of different tested ink formulations.

	Ink a	Ink b	Ink c	Ink d
Water	91	91	48	23
Dispersant	2	1	1	1
PnP	5	5	5	5
PG	0	0	45	70
ALA	0	2	0	0
MWCNT	2	1	1	1
Viscosity	5.8	36	9.9	34

ics (10–200 mPa·s) [30,31]. From literature it is known that the observed effect is related to the liquid transfer mechanism, which, for low viscosity liquids, does not happen as single droplets, but with a continuous fluid meniscus. This meniscus spreads over the gravure cells and accumulates the ink during printing, it is finally abandoned at the end of the gravure relief and squeezed out by the non-engraved surface of the gravure cylinder [32]. Therefore, two approaches were chosen to increase the viscosity of the ink. In the first one the viscosity was increased by a thickening agent (Borchi® Gel ALA). Thereby the issue of ink excess could be eliminated. But as it can be seen in Fig. 4b, the higher viscosity resulted in an inhomogeneous layer due to the effect of viscous fingering. This is a well-known phenomenon which is often observed during the deposition of thin films by gravure printing. The reason for it is an inhomogeneous ink splitting between printing plate and substrate due to fluid dynamic instabilities (Saffman–Taylor Instability). These instabilities finally result in thickness undulations within the deposited ink layer. Therefore, if the drying time (solidification) of the ink is shorter than the leveling-time of these inhomogeneities, they will be preserved on the final electrode [32–34]. This issue could finally be circumvented by the addition of a viscous high boiling point co-solvent propylene glycol (PG) (see Section 2.1). The advantage of such solvent is that it increases the viscosity and at the same time extends the drying time of deposited liquid film. Therefore, PG promotes ink leveling and hence uniform film formation. By gradual increase of PG content, optimal printing results were finally found at a concentration of 70 wt% PG (see Fig. 4c,d). The composition and the viscosity of the described above inks is summarized in Table 1. The letters that designate the inks correspond to the respective pictures in Fig. 4.

### 3.1.1. Contact angle and plasma treatment

Ink d (see Table 1 and Fig. 4d) has surface tension of 34.6 mN/m giving a contact angle of about 21° on a 3 s plasma treated PDMS film. Without plasma treatment the contact angle is above 75° which is too high for printing. According to the work of N. Bornemann [34] it should not exceed ~40° and drop below ~5° for adequate printing. As showed in Fig. 5, there is a surface energy saturation of the plasma treated PDMS film at about 75 mN/m which is reached after a treatment time of about 10 s. In order to print uniformly at least 2 s plasma treatment was needed. Shorter treatment times led to discontinuous and, therefore, hence non-conducting electrodes.

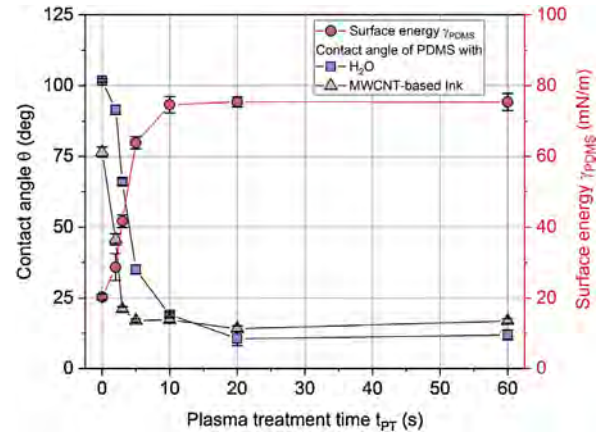


Fig. 5. Contact angle and PDMS surface energy as function of plasma treatment time.

Table 2

Properties of the gravure printed electrodes.

Electrode type	Gravure cell depth, $\mu\text{m}$	Gravure cell volume, $\text{ml}/\text{m}^2$	Thickness, nm	Initial sheet resistance $R_0$ , $\text{k}\Omega$
Thin	8	6	$55 \pm 13$	$13.7 \pm 1.6$
Middle	16	11.4	$115 \pm 7$	$4.5 \pm 0.4$
Thick	24	15.7	$150 \pm 11$	$2.5 \pm 0.7$

### 3.2. General characterization of gravure printed electrodes

Besides the ink properties, the final printing results depend on the process parameters. Special attention should be given to an appropriate ink dosing and transfer. In contrast to conventional graphical printing, where a picture is built up by patterns of single isolated drops (pixels), the deposited layer should form a continuous uniform coating. This can be achieved by choosing an appropriate engraving of the printing cylinder. In this regard, two important parameters are the cell volume, which determines the amount of liquid that is transferred by a single cell, and the line screen, which corresponds to the number of cells for a given distance. From literature it is known that too large cells can result in ink excess leading to diffuse borders and large thickness undulations [32]. Too small cells on the other hand, can result in incomplete ink covering. To a certain extent, this issue can be circumvented by increasing the cell density. However, it is known that a smaller cell volume is not always beneficial because smaller cells are more likely to clog, which finally lowers the printing reliability. Within the scope of this study, the patterns on the printing cylinder had an engraving of 120 lines/cm. The cell depths of the main pattern were 8  $\mu\text{m}$ , 16  $\mu\text{m}$  and 24  $\mu\text{m}$  which resulted in electrodes of three different thicknesses (see Fig. 6, left and Table 2). Smaller cell volumes lead to incomplete coverage because the transferred ink drops are too small for the formation of a continuous liquid layer. This behavior is shown in the right image of Fig. 6. The image shows 15 printing fields of different cell volumes. The top three fields have the same engraving as the main patterns which corresponded to a cell volume of 6  $\text{ml}/\text{m}^2$ , 11.4  $\text{ml}/\text{m}^2$  and 15.7  $\text{ml}/\text{m}^2$  from left to right. In vertical direction from top to down, the cell depths were constant

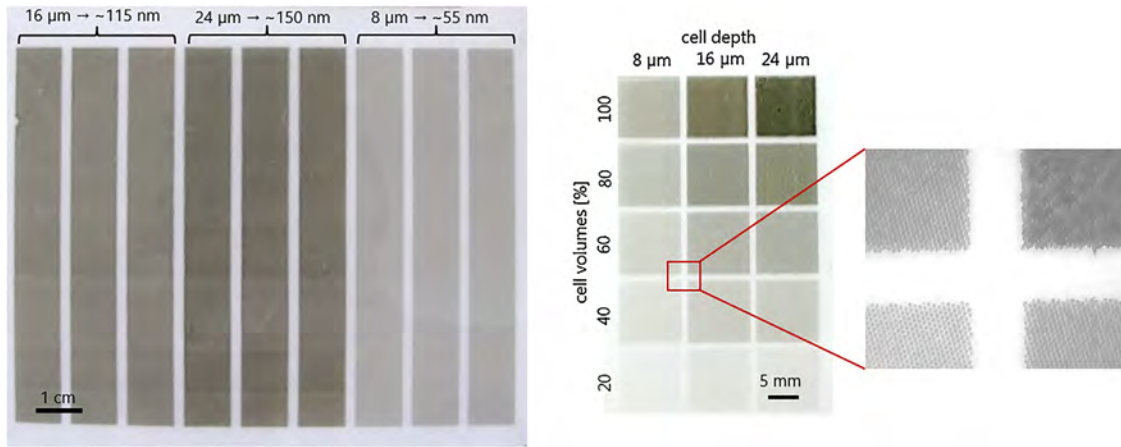


**Fig. 6.** Images of the printing results. Left: Pattern that were used for electro-mechanical characterization. Right: 15 printing fields of different cell volumes. Note that below a certain cell volume the transferred drops do not coalesce and therefore no continuous layer can be formed.

and the opening widths of the cells were varied in such a way that the cell volumes were gradually decreased from 100% to 20%. As it can be seen in the magnification inset, the cell volumes below 60% at 8 μm cell depth resulted in single drop transfer and, therefore, incomplete electrode coverage. However, not only the cell volume had an influence on the printing results but also the ratio of cell depth to opening width. As an example, the field “8 μm/60%” with a cell volume of 2.2 ml/m<sup>2</sup> was electrical conductive, whereas the field “16 μm/40%” with 2.4 ml/m<sup>2</sup> cell volume did not show any conductivity. This indicates a lower liquid transfer ratio for smaller cell openings which is a commonly seen behavior in gravure printing processes [32].

Printing speed is another important process parameter which affects the layer formation. Therefore, three different printing speeds (300 mm/s, 500 mm/s, and 1000 mm/s) were evaluated. However, in regard to morphology and conductivity no significant difference could be observed in this range. For further investigation the printing speeds 500 mm/s was chosen.

### 3.3. Optical properties and percolation behavior

The printed electrodes are optically transparent, exhibiting a transmittance of 73% at the thickness of 55 nm, measured at a wave length of 550 nm. This feature is particular interesting for optical applications of DEA's like adaptive lenses or displays [12,35]. From literature [36] it is known that for conductive bulk-like films, the relation between transmittance  $T$  and sheet resistance  $R_s$  can be expressed as:

$$T = \left[ 1 + \frac{Z_0}{2R_s} \frac{\sigma_{op}}{\sigma_{dc}} \right]^{-2} \quad (1)$$

where,  $Z_0$  is the impedance of free space (377 Ω),  $\sigma_{dc}$  the bulk conductivity and  $\sigma_{op}$  the optical transparency which is related to the absorption coefficient  $\alpha$  as  $\sigma_{op} = \alpha/Z_0$ . The Eq. (1) is appropriate for bulk-like behavior when the conductivity is independent from the layer thickness. However, if the thickness of the MWCNT layer is reduced below a critical value  $t_{min}$ , the relation undergoes a transition from bulk to percolative behavior. In this regime the electrode material does not cover the entire surface of the film (see Fig. 7) and the electrical conductivity becomes smaller than the conductivity in the bulk regime. The percolation theory states a non-linear power law dependency of the conductivity on the thickness as  $\sigma_{dc} \propto (t - t_c)^n$  where  $t_c$  is the thickness corresponding to the percolation

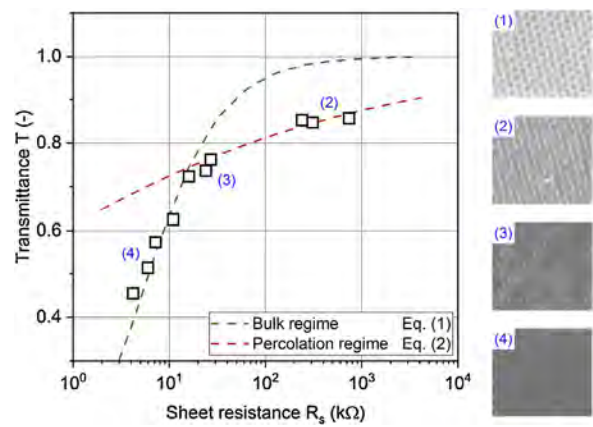


**Fig. 7.** Transmittance at 550 nm as a function of sheet resistance for the printed electrodes. The data can be divided in two regimes: percolation regime and bulk regime. The optical microscope images on the right show the corresponding surface morphologies of the printed layers (1.2 mm x 1 mm). The point corresponding to image (1) is not reported in the graph as this layer was not electrically conductive.

threshold. This leads to a new relation between  $T$  and  $R_s$  for thin, transparent and conductive networks:

$$T = \left[ 1 + \frac{1}{\Pi} \left( \frac{Z_0}{R_s} \right)^{1/n + 1} \right]^{-2}, \quad \Pi = 2 \left[ \frac{\sigma_{dc}/\sigma_{op}}{(Z_0 t_{min}\sigma_{op})^n} \right] \quad (2)$$

### 3.4. Electromechanical performance

#### 3.4.1. Uniaxial electro-mechanical characterization

When subjected to tensile straining, the resistance of the electrode increases. In order to characterize the printed electrodes and to understand the changes of their morphology, the uniaxial tensile straining was carried out. In Fig. 8 the sheet resistance of the electrodes printed on PDMS films with different plasma treatment times is presented as a function of uniaxial strain.

As expected, the sheet resistance increases with increasing strain. The electrodes printed on PDMS that was plasma treated for 2 s and 5 s behave quite similar and exhibit gradual increase of sheet resistance within the whole tested strain range. However, with increased plasma treatment time the progressive increase in sheet resistance is observed. In order to investigate the nature of this behavior change the strained samples were fixed on the microscope slide at the end of each test and investigated under the optical microscope (see Fig. 8). Obviously, and extensive cracking of PDMS

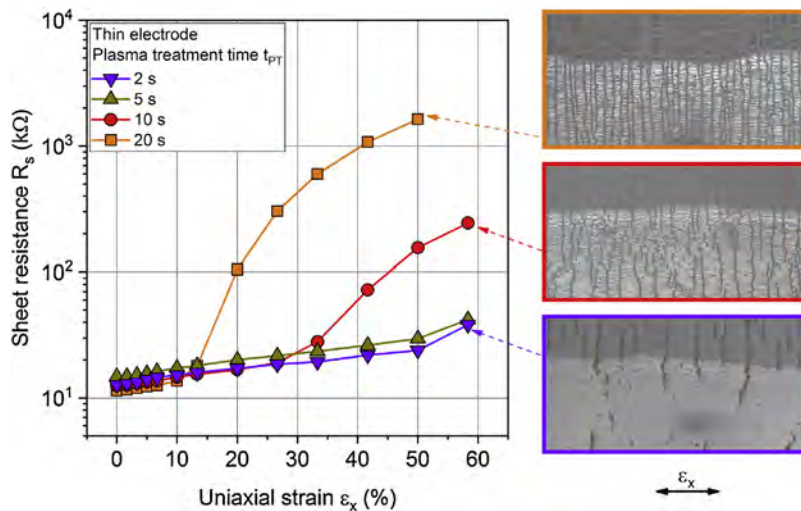


**Fig. 8.** Electro-mechanical behavior of thin electrode printed on PDMS film subjected to different plasma treatment times and the morphology of the strain electrodes. Size of micrographs  $200 \times 100 \mu\text{m}$ .

surface and the deposited electrode is responsible for the dramatic loss of conductivity. The reason for the cracking of PDMS surface is probably silica-like layer that under certain conditions can be created during plasma treatment.

The effect of plasma treatment on a PDMS surface is well known [37] [38]. Oxygen radicals react with methyl groups of the PDMS chains and convert them into silanol groups. This causes an increase of the surface energy of PDMS, and it becomes hydrophilic. However, these reactive silanol groups can react with other silanol groups in the vicinity and result in condensation reaction forming covalent Si-O-Si bond. If the PDMS surface is subjected to high doses of plasma, it can result in formation of a superficial silica-like layer. This layer is considerably stiffer than PDMS and is highly brittle. Hence, when a PDMS with the silica-like layer is strained, the latter is able to accommodate substantially less deformation than the former, which leads to nucleation and lateral propagation of cracks in the silica-like layer, usually throughout its whole thickness [39]. As it is shown in Fig. 8, these cracks can also propagate into the electrode and significantly influence its electro-mechanical behavior.

The obtained value of the electrical resistance for the electrode printed on the PDMS film plasma treated for 2 s under uniaxial straining of 50% is  $\sim 24 \text{ k}\Omega$ , which corresponded to 90% increase of the initial resistance. For comparison, at the same strain values the 60% increase of resistance was reported in [40]. However, it should be noted that the electrode in the mentioned study was spray-deposited with single-wall carbon nanotubes with the average length of 2–3  $\mu\text{m}$  and, as a consequence higher aspect ratio. This may explain somewhat better performance.

The density of cracks increases with increasing time of plasma treatment. Moreover, a pronounced wrinkling perpendicular to the direction of straining is observed on the electrode printed on PDMS film subjected to 10 s and 20 s plasma treatments. This wrinkling is caused by contraction strain and can be seen both on PDMS surface as well as the electrode. The electrode printed on PDMS film plasma treated for 2 s exhibits significantly smaller cracking under the same amount of straining, both on the PDMS surface and electrode itself (see Fig. 8). Notably, not all the cracks in the surface of PDMS are transferred onto the electrode. This may be caused by the stiffening effect of the electrode. Besides that, no wrinkling due to contraction was observed, which indicates the absence of the brittle silica-like layer.

The influence of the electrode thickness on its relative resistance change is presented in Fig. 9. All three types of electrodes exhibit similar behavior until straining up to 33%. Under further straining middle and thick electrodes start to lose their conductivity more rapidly, while thin electrode continues to exhibit gradual linear increase in resistance.

The morphology of the strained thin and thick electrodes is presented in Fig. 9. The thick electrode exhibits more pronounced cracking than the thin one. This effect occurs due to the increased stiffness as the electrodes get thicker. The stiffer electrodes can accommodate smaller deformations while maintaining their integrity. Based on better electro-mechanical performance of the thin electrodes we decided to use that type for further investigations.

After investigating the strained thin electrode, it was unfixed from the microscope slide, fully unloaded, and examined in the relaxed state (see Fig. 9). A pronounced wrinkling of the electrode was observed, indicating the change in morphology caused by straining. It is plausible to assume that this would affect the electro-mechanical behavior of the electrode under further repeated straining. In order to investigate this effect a cyclic uniaxial strain increased test was performed on the electrodes printed on PDMS films plasma treated for 2 s and 20 s (Fig. 10(a) and (b) respectively).

During the first straining cycle 0→5→0% both electrodes showed similar response with gradual linear resistance increase to straining within this range. After unloading, a small rise in initial sheet resistance was observed. This change could have been caused by the minor rearrangements within the MWCNT layers, which aligned themselves in the direction of straining. Similar effect was reported in [40].

As the electrodes were subjected to second straining cycle 0→20→0%, they demonstrated similar electro-mechanical behavior as was showed earlier in Fig. 8, i.e. at  $\epsilon_x \approx 10\%$  the electrode printed on PDMS film that was plasma treated for 20 s demonstrated a pronounced progressive increase in resistance, while the other one showed gradual sheet resistance rise. Upon unloading both electrodes exhibited pronounced hysteresis. The electrode printed on PDMS film plasma treated for 2 s underwent gradual decrease of resistance. At the same time, the electrode printed on PDMS film plasma treated for 20 s demonstrated change in behavior during the decrease of resistance upon unstraining. In the range

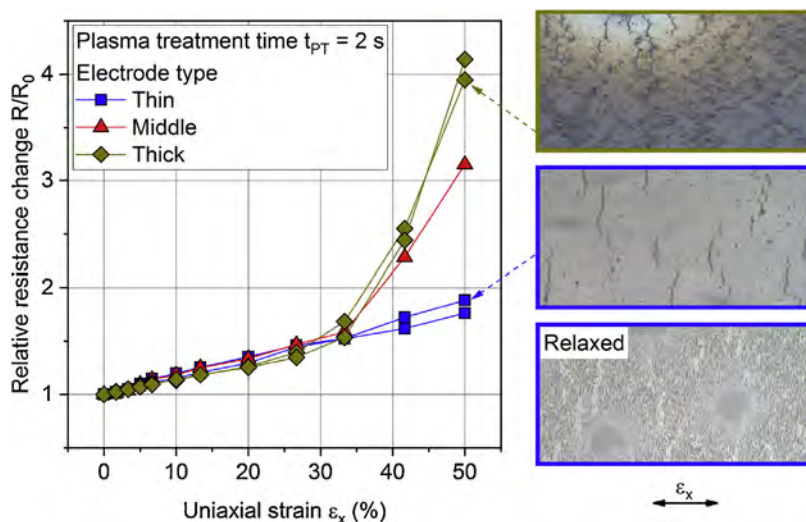


Fig. 9. Electro-mechanical behavior of the electrodes of different thicknesses and morphology of strained and relaxed electrodes. Size of micrographs  $200 \times 100 \mu\text{m}$ .

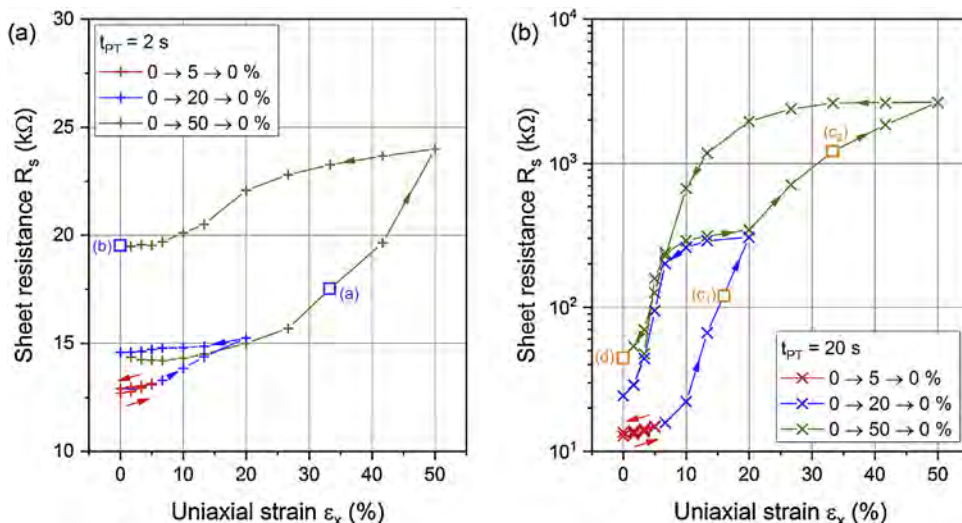


Fig. 10. Results of cyclic uniaxial strain increased test on the electrodes printed on PDMS films plasma treated for 2 s (a) and 20 s (b). Different shapes of hysteresis loops indicate different mechanisms that influence electromechanical behavior of the electrodes.

20→10% the electrode recovered gradually. However, during further unloading (10→0%) the resistance decreased more rapidly.

During the third straining cycle 0→50→0% the electro-mechanical behavior of the investigated electrodes followed the same pattern as during the second cycle 0→20→0%. Naturally, the maximal resistance values increase correspondingly higher as the response to higher degree of straining, making the hysteresis even more pronounced. Due to distinct differences in the measured hysteresis loops it is obvious that different mechanisms must be responsible for such significant discrepancies in electro-mechanical behavior. In order to obtain better understanding of the morphological changes upon straining and unloading the electrodes were observed with the SEM. The samples of the electrodes were observed in initial, strained and relaxed states (Fig. 11). The investigated states are also indicated in Fig. 10 with corresponding symbols.

Based on the obtained experimental data, as well as other reported investigations [40,41], the following two distinctive mechanisms are proposed to explain the hysteresis, as well as the differences in electro-mechanical behavior of two electrodes,

printed on the PDMS films subjected to 2 s and 20 s plasma treatment respectively.

**3.4.1.1. Morphology change driven hysteresis.** It is hypothesized that the hysteresis is caused due to an alteration of the electrode morphology during elongation and contraction.

As the strain  $\varepsilon_x$  is applied, the electrode and the PDMS film are subjected to the same loading. Consequently, the viscoelastic PDMS film stretches in the direction  $\varepsilon_x$  and contracts in  $\varepsilon_y$  (Poisson-effect), accumulating elastic energy. However, the electrode accommodates the imposed tensile deformation in a different way: the MWCNTs tend to rearrange and align themselves in the direction of the tensile strain. Therefore, the electrode layer as whole undergoes kind of “plastic” deformation. This means that the electrode experiences a change of its inherent morphology, analogically to the rearrangement of polymer chains during the plastic deformation of thermoplastics (e.g. polypropylene).

Nevertheless, the electrode remains conductive, and this rearrangement manifests itself as a liner increase of sheet resistance during straining. Although some very localized and limited cracking

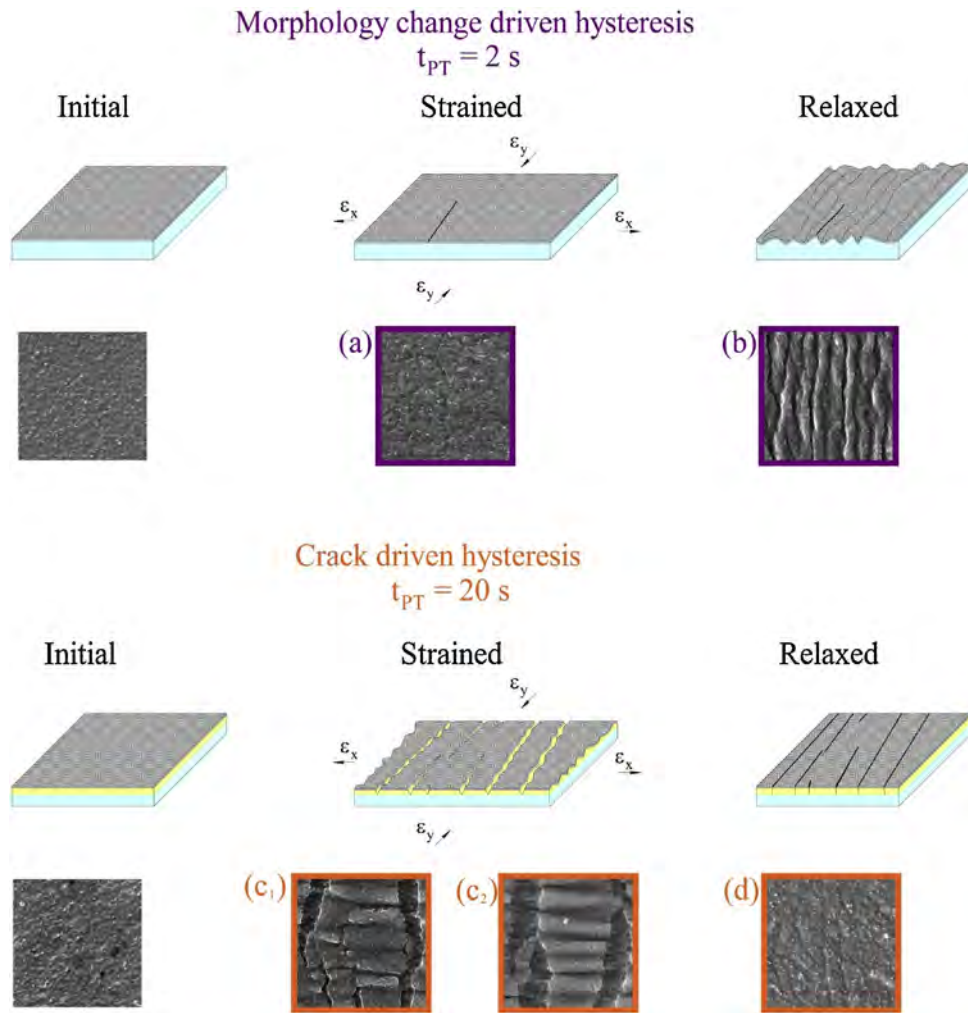


**Fig. 11.** Explanation of the morphology change driven hysteresis and the crack driven hysteresis. Size of the SEM micrographs  $8 \times 8 \mu\text{m}$ .

may be observed at high strain levels (see Fig. 11(a)), the electrode to a greater extent maintains its integrity.

Upon unloading, the PDMS film starts to contract in the direction opposite to  $\epsilon_x$  due to the stored elastic energy. But, as a result of rearrangement of MWCNTs during prior tensile straining, the electrode is now subjected to compression. Due to high stiffness of MWCNTs, the electrode has poor ability to sustain compressive strains and cannot reverse the morphology changes to the inherent state due to above mentioned ‘plastic’ deformation. Therefore, it buckles and forms wrinkles in the direction of unloading in order to accommodate the compressive deformation (Fig. 11(b)). This change of morphology during stretching and the inability to reverse it during contraction is also reflected in the electrical resistance response. During unloading the resistance is significantly less susceptible to the changes of strain with comparison to its responsiveness during initial straining. Therefore, after the completion of the straining-unloading cycle, as the result of the morphology driven hysteresis, the electrode in the relaxed (i.e. fully unloaded) state exhibits higher resistance than before (see Fig. 10(a)).

Provided that the repeated uniaxial tensile strain doesn’t exceed the highest strain during the first cycle, the electro-mechanical behavior of the electrode is now nominally stabilized. Thus, the response of the resistance on imposed strain should be the same both straining and unloading. It follows a similar path that occurred during the unloading in the first cycle. It is worth noting that the high number of repeated cycles might alter this stable electro-

mechanical behavior. However, no investigations in this regard were carried out within the scope of this study.

An interesting effect was observed during repeated tensile straining  $0 \rightarrow 50\%$  (see Fig. 10(a)): a slight decrease of electrical resistance as a reaction to an increased strain until 5%. Most probably this happened as a result of flattening out of the wrinkles, which created more contact points between MWCNTs causing a small increase in conductivity. Similar effect was observed during biaxial straining of this electrode and will be addressed later in this paper.

The described mechanism of morphology change driven hysteresis occurs only if the PDMS film is homogeneously compliant. But, as it was mentioned before, the silica-like layer on the surface of PDMS film is very brittle. Therefore, a different model is needed to explain the electro-mechanical behavior of the electrodes that were deposited on PDMS films subjected to prolonged plasma treatment.

**3.4.1.2. Crack driven hysteresis.** This mechanism anticipates deterioration of integrity of both electrode and the surface layer of the PDMS film when subjected to tensile straining.

The electro-mechanical response of the electrodes printed on PDMS films that were subjected to prolonged plasma treatments (e.g. 10 s in Fig. 8, as well as 20 s in Figs. 8 and 10) is characterized by two zones: before and after reaching a critical strain. In the first zone, the electro-mechanical behavior of the electrode is the same as it was described before. However, after reaching the critical strain (8–12% for the electrode printed on the PDMS film

plasma treated for 20 s) a progressive rise in sheet resistance is observed. The SEM investigations showed (Fig. 11(c<sub>1</sub>)) that above this strain an extensive network of cracks in the PDMS surface and the electrode is generated. The reason for this is the brittle silica-like layer on the PDMS surface: it can't accommodate the imposed tensile deformation and starts to crack mostly perpendicular to the direction of strain  $\varepsilon_x$ . It is plausible to assume that the cracking occurs throughout the whole thickness of the silica-like layer and induces cracking of the electrode. The MWCNT electrode cannot sustain such highly localized strain levels induced by the crack formation. This severely deteriorates its integrity, which in its turn, causes a dramatic increase in electrical resistance. Besides that, the silica-like layer together with the electrode starts to wrinkle in the direction perpendicular to cracking. It should be noted, that this wrinkling is of a different nature than the one described before for the morphology change driven hysteresis. Here, the wrinkling is caused due to the accommodation of the compressive contraction strain  $\varepsilon_y$  as a result of Poisson ratio mismatch between silica-like layer and PDMS as described in literature [39]. As a consequence, the electrode morphology is altered as well. In contrast, during the morphology change driven hysteresis the wrinkling is caused by the electrode upon unloading, and the PDMS surface follows this wrinkling deformation parallel to the direction of straining-unloading.

As the strain increases, more cracks are being nucleated, while already existing cracks become wider (Fig. 11(c<sub>2</sub>)) in the direction of straining and also propagate in the lateral direction perpendicular to the imposed tensile strain  $\varepsilon_x$ . This causes even higher deterioration of the electrode. Besides that, the amplitude of wrinkling increases as a response to the increasing contraction strain  $\varepsilon_y$ .

Similar to straining, two regions of the resistance-strain response can be distinguished during unloading and associated with it resistance drop. As the axial strain is removed, the PDMS film starts to contract as a result of accumulated during straining elastic energy.

This causes narrowing of the cracks and decrease in the amplitude of wrinkles. The electrode resistance doesn't follow the same path as during straining, causing hysteresis. The conductivity recovers fairly slowly during this process. However, at a certain strain the cracks start to close and create more passes for the current. This is followed by a dramatic decrease in electrical resistance. Referring to the results in Fig. 10(b), this happened around 8–10% for the unloading 20→0%, and between 10–20 % for 50→0%.

When the electrode with the PDMS film is completely unloaded, no open cracks could be found. However, due to the severe deterioration of integrity under straining, the traces of the cracks can be observed (Fig. 11(d)) in relaxed state. This causes the increase in sheet resistance compared to the initial state. Parallel to the crack narrowing and closure, the wrinkling also disappears, as the contraction strain decreases, causing the electrode to flatten out.

If the tensile strain is reapplied, the resistance-strain response follows the same pattern as during the unloading (see Fig. 10(b), unloading 20→0% and straining 0→50%). This indicates that the same mechanism controls the electro-mechanical behavior of the electrode during both straining and unloading, just in the inverted order.

#### 3.4.2. Biaxial electromechanical characterization

During its operation, the EAP transducer contracts, which creates a biaxial tensile straining in the plane perpendicular to the axis of contraction. This poses a necessity to understand the electro-mechanical behavior of the electrodes printed on PDMS films under the conditions of biaxial straining.

In this section we report and discuss the experimental results of biaxial straining of thin electrodes printed on the PDMS film subjected to different plasma treatment times in the range  $t_{PT} = 2-60$  s. At the end of each test, while the electrodes were subjected to max-

imal biaxial strain, they were glued to the ring holders. This allowed us to analyze the morphological states of the strained electrodes with the AFM.

In Fig. 12 the electro-mechanical behavior of the electrodes that were printed on the PDMS films plasma treated for 2, 20 and 60 s is presented. In total, six strain cycles were performed on each sample. Together with the relative resistance change as a function of biaxial strain, the corresponding AFM scans are presented.

The electrodes printed on the PDMS films that were subjected to plasma treatment for 2 s and 20 s endured two first straining cycles (i.e. 0–0.8 N loading) with neither increase in initial resistance, nor any pronounced hysteresis. The first electrode performed somewhat better, as it exhibited less steep resistance-strain response. However, the electrode printed on the PDMS film plasma treated for 60 s showed the increase of the initial resistance already after the first cycle, with a clear presence of hysteresis. This indicates that with plasma treatment of the PDMS film for 60 s, the electrode can already be degraded at a fairly small strain values. At the same time, in the other electrodes that are presented in Fig. 12, no cracks are generated during biaxial straining within this strain range (i.e. 0–0.8 N loading).

During the second and the third stage of biaxial straining (i.e. cycles with 0–1.5 N and 0–2.2 N loading respectively) the electrode printed on the PDMS film plasma treated for 2 s exhibits the morphology driven hysteresis, the mechanism of which was described above. The AFM investigations confirmed almost crack-free electrode. Note a small decline of resistance with increasing biaxial strain during the second cycle of the loading 0–2.2 N. The possible reason for this behavior is explained previously. However, during biaxial straining, this effect is more pronounced.

At the same time, the electrode printed on the PDMS film plasma treated for 60 s demonstrated clear crack driven hysteresis behavior for the following straining cycles. The AFM examinations revealed severe cracking of the electrode and the PDMS surface due to the presence of the silica-like layer. Due to biaxial straining two groups of cracks, each perpendicular to the strain that induced them, can be distinguished.

Let's consider now the electro-mechanical behavior of the electrode printed on the PDMS film plasma treated for 20 s. On one hand side, the behavior of the resistance-strain curves upon straining corresponds fairly well to those, expected during the crack driven hysteresis. On the other hand, the measured resistance changes during biaxial straining are significantly smaller than those measured in uniaxial testing of the same electrode. The AFM investigations (see Fig. 12(b)) confirmed the cracking of the electrode, strongly indicating that the electrode exhibited crack driven hysteresis. Naturally, the question arose: why was the electrode still capable of conducting the current?

A distinctive feature of the AFM scans in Fig. 12(b) on the contrary to the micrographs in Fig. 11(c<sub>1</sub>) and (c<sub>2</sub>) is the absence of wrinkling of the silica-like layer on the PDMS surface (and subsequently the electrode). Indeed, during biaxial deformation there is no contraction strain in the plane of the electrode (i.e. no strain  $\varepsilon_y$  in the Fig. 11), therefore the wrinkling of the silica-like layer doesn't occur. This effect ensures that the electrode remains flat upon biaxial straining. Because of significantly less pronounced topology of the electrode, it is plausible to assume that the MWCNTs of the electrode can bridge over the cracks as they nucleate and get wider, providing electrical conductivity. This bridging effect was confirmed by the AFM measurements (see Fig. 14). Naturally, when the cracks get wider, the bridging effect deteriorates, as the MWCNTs are too short to be able to span over them. This statement is supported by the AFM scan of the electrode printed on the PDMS film plasma treated for 60 s (Fig. 14), where no bridging was observed over the significantly wider crack.

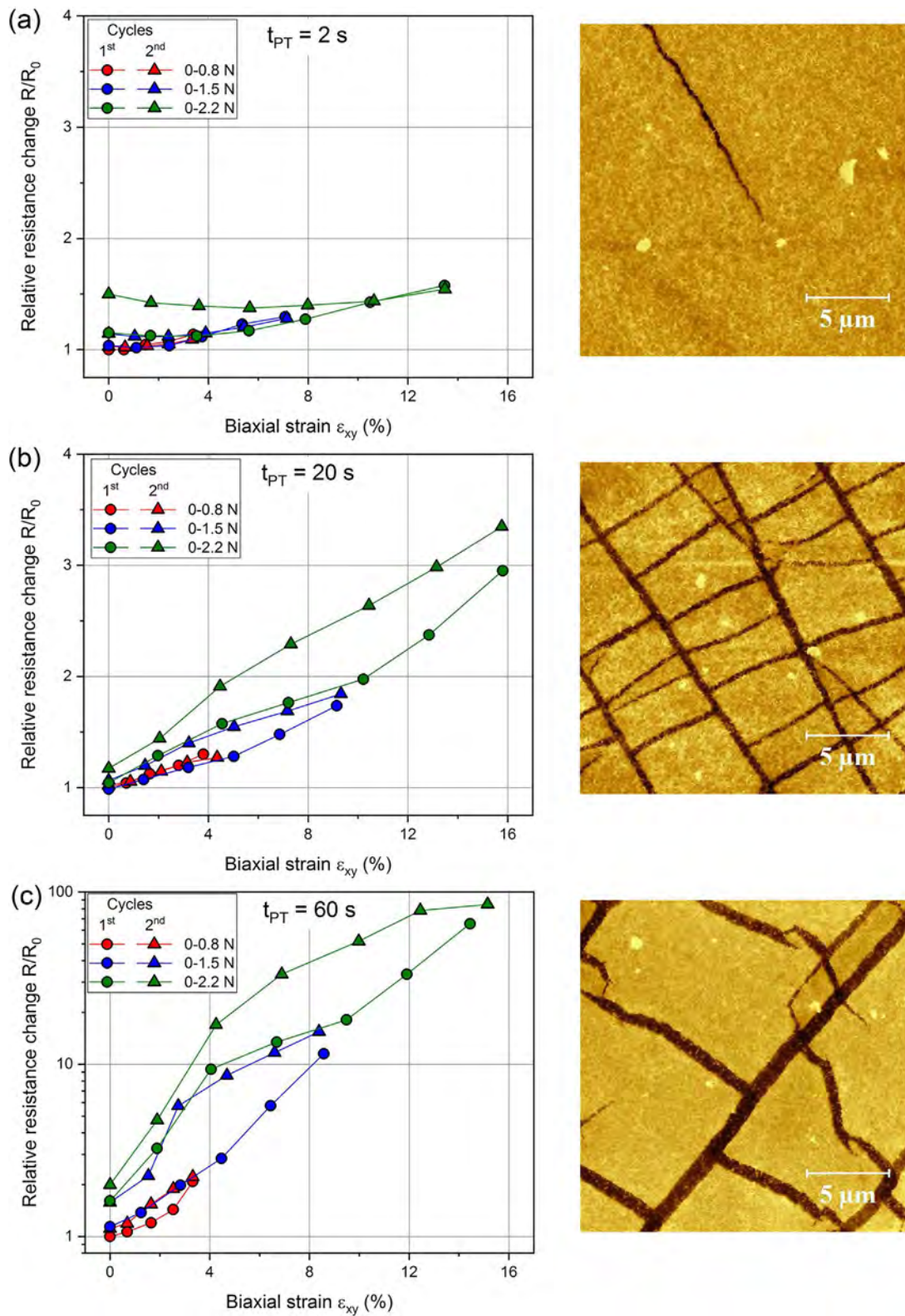


**Fig. 12.** Electro-mechanical behavior of MWCNT electrodes printed on PDMS films plasma treated for 2 s (a), 20 s (b) and 60 s (c). The AFM scans on the right show the electrode surface at the end of all six straining cycles.

By comparing the relative increase in resistance for electrodes printed on the PDMS films that were subjected to different plasma treatment time under the same biaxial strain of 4%, 8%, and 12%, a clear correlation between plasma treatment time and relative resistance increase can be demonstrated (Fig. 13). Obviously, the

electrodes printed on PDMS films undergoing short plasma treatment time are capable of accommodating larger biaxial strain without a dramatic impact on the resistance.

As it is shown in Fig. 12, decreasing the dose of plasma treatment has an impact on the density of cracks, resulting in bigger

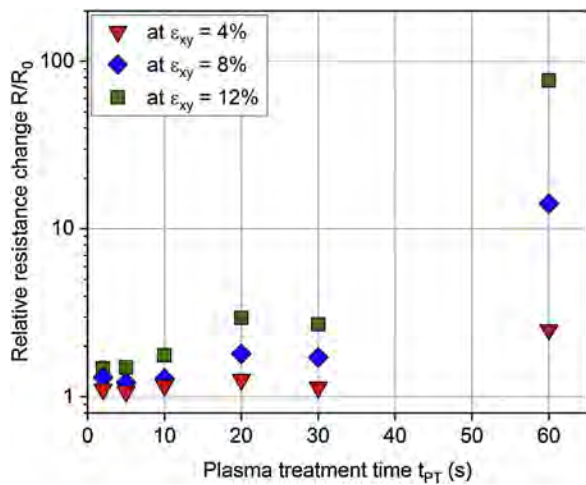


**Fig. 13.** Relative resistance change as a function of plasma treatment time at defined biaxial strain states.

island for longer plasma treatment times. This can be associated with the fact that the plasma treatment time is proportional to

thickness of silica-like layer. Upon straining of the PDMS film with the thick silica-like layer on the surface, the cracking occurs even under relatively low strains. Subsequently, the further applied deformation is accommodated rather by widening of those cracks rather than nucleating new, making a strain range of crack nucleation rather small. On the other hand, the thinner silica-like layer provides a broader strain range of crack nucleation, which promotes formation of denser net of cracks.

In order to verify this statement, a high resolution detailed AFM scanning of the electrodes from Fig. 12 were carried out and are presented in Fig. 14. Considering that the electrodes were fixed on the frames while being subjected to the same biaxial strain, the cracks should also be narrower. This is demonstrated by profiles that were extracted from the detailed scans perpendicular to the cracks. From these profiles it is also clearly seen that the cracks not only get wide, but also deeper as the plasma treatment time of PDMS films increases. This is consistent with the fact that higher plasma treatment doses generate thicker silica-like layers [42,39].

The cracks were measured by extracting profiles from the AFM scans perpendicular to the cracks, and their depth was estimated as a vertical distance between the average surface of the electrode and the lowest point in the groove from the crack. The results are reported in Fig. 15 are averaged values based on the analysis of five

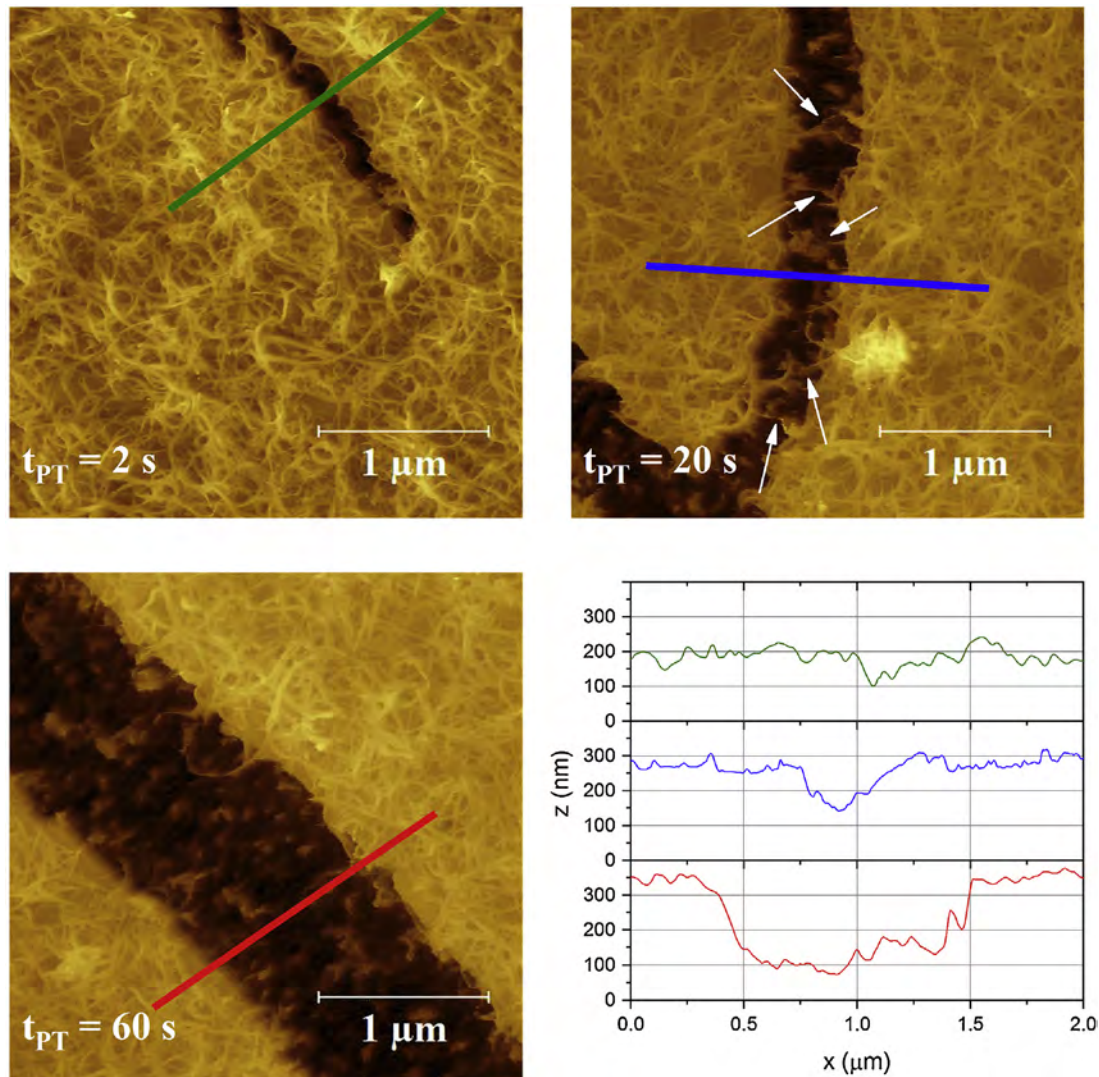


**Fig. 14.** Detailed AFM scans of cracks in the electrodes subjected to different plasma treatment times with the corresponding profiles across the cracks. The MWCNT-bridging over the cracks is indicated with white arrows.

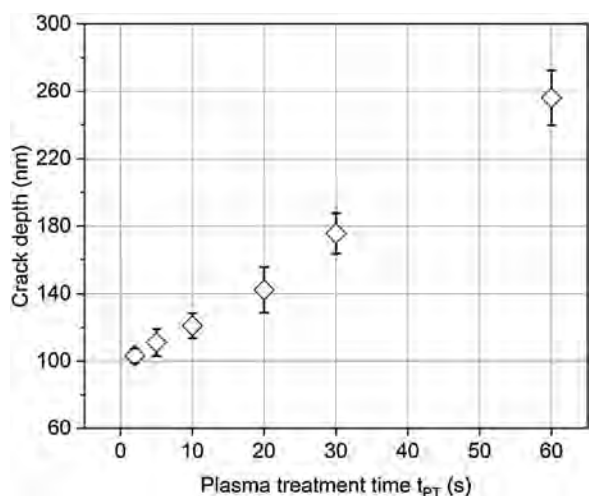


Fig. 15. Cracks depth as a function of plasma treatment time. Note that the electrode thickness is  $\sim 55$  nm.

different profiles per scan of the electrodes printed on the PDMS films subjected to different plasma treatment time.

Obviously the crack depth increases with increased plasma treatment time. This confirms the increased thicknesses of silica-like layers for longer plasma treatment time of the PDMS films.

#### 4. Conclusions

In this work we investigated the gravure printing method for large-area and continuous MWCNT-based electrode deposition on thin PDMS films. For this purpose the MWCNT-based ink was developed and its properties were tailored to ensure stable and high quality printing results.

The influence of printing parameters, such as printing speed, cells volume, and plasma treatment time, on the electrode morphology and its electro-mechanical behavior was investigated. By varying the process parameters we were able to produce and examined the electrodes in a range of thicknesses between 55 nm and 150 nm.

A special attention was addressed to the morphological changes of the electrodes subjected to uniaxial and biaxial straining. Two mechanisms of the electrode behavior change were proposed and experimentally supported. It was shown that the brittle silica-like layer on the surface of PDMS plays a crucial role in governing the electro-mechanical behavior of the electrode. The results proved that the thickness of the silica-like layer increases with the plasma treatment time.

To our knowledge, this work is the first describing a robust industrial process for printing compliant electrodes on PDMS films, opening the doors to mass production of elastomeric transducers or sensors.

#### Acknowledgement

The authors gratefully acknowledge the financial support by the Swiss Commission for Technology and Innovation (CTI - Projekt-Nr. 18422.1 PFIW-IW).

#### References

- [1] F. Carpi, D. De Rossi, R. Kornbluh, R. Pelrine, P. Sommer-Larsen, *Dielectric Elastomers as Electromechanical Transducers*, Elsevier Ltd., 2008.
- [2] T. Takahashi, K. Takei, A.G. Gilies, R.S. Fearing, A. Javey, Carbon nanotube active-matrix backplanes for conformal electronics and sensors, *Nano Lett.* 11 (12) (2011) 5408–5413.
- [3] T. Sekitani, T. Someya, Stretchable, large-area organic electronics, *Adv. Mater.* 22 (2010) 2228–2246.
- [4] R. Perline, R. Kornbluh, Q. Pei, J. Joseph, High-speed electrically actuated elastomers with strain greater than 100%, *Science* (2000) 836–839.
- [5] G. Kovacs, L. Duering, S. Michel, G. Terrasi, Stacked dielectric elastomer actuator for tensile force transmission, *Sens. Actuators A* 155 (2009) 299–307.
- [6] K. Xie, B. Wei, Materials and structures for stretchable energy storage and conversion devices, *Adv. Mater.* 26 (2014) 3592–3617.
- [7] Y. Bar-Cohen, *Electroactive Polymer (EAP) Actuators as Artificial Muscles - Reality, Potential, and Challenges*, 2nd edition, SPIE, Ipswich, MA, 2011.
- [8] P. Brochu, Q. Pei, Advances in dielectric elastomers for actuators and artificial muscles, *Macromol. Rapid Commun.* 31 (2010) 10–36.
- [9] T. Smela, Conjugated polymer actuators or biomedical applications, *Adv. Mater.* 15 (6) (2003) 481–494.
- [10] S. Michel, X.Q. Zhang, M. Wissler, C. Loewe, G. Kovacs, A comparison between silicone and acrylic elastomers as dielectric materials in electroactive polymer actuators, *Polym. Int.* 59 (3) (2010) 391–399.
- [11] C. Loewe, X. Zhang, G. Kovacs, Dielectric elastomers in actuator technology, *Adv. Eng. Mater.* 7 (5) (2005) 361–367.
- [12] S. Rosset, H.R. Shea, Flexible and stretchable electrodes for dielectric elastomer actuators, *Appl. Phys. A* 110 (2013) 281–307.
- [13] J. Song, Mechanics of stretchable electronics, *Curr. Opin. Solid State Mater. Sci.* 19 (3) (2015) 160–170.
- [14] J.A. Rogers, T. Someya, Y. Huang, Materials and mechanics for stretchable electronics, *Science* (2010) 1603–1607.
- [15] S. Yao, Y. Zhu, Nanomaterial-enabled stretchable conductors: strategies, materials and devices, *Adv. Mater.* 27 (9) (2015) 1480–1511.
- [16] S. Shang, W. Zeng, X.-M. Tao, High stretchable MWNTs/polyurethane conductive nanocomposites, *J. Mater. Chem* 21 (2011) 7274–7280.
- [17] C.W. Park, S.W. Jung, S.C. Lim, J.-Y. Oh, B.S. Na, S.S. Lee, H.Y. Chu, J.B. Koo, Fabrication of well-controlled wavy metal interconnect structures on stress-free elastomeric substrates, *Microelectron. Eng.* 113 (2014) 55–60.
- [18] N. Lambrecht, T. Pardoën, S. Yunus, Giant stretchability of thin gold films on rough elastomeric substrates, *Acta Mater.* 61 (2013) 540–547.
- [19] D.-H. Kim, J. Xiao, J. Song, Y. Huang, J.A. Rogers, Stretchable, curvilinear electronics based on inorganic materials, *Adv. Mater.* 22 (2010) 2108–2124.
- [20] K.-Y. Chun, Y. Oh, J. Rho, J.-H. Ahn, Y.-J. Kim, H.R. Choi, S. Baik, Highly conductive, printable and stretchable composite films of carbon nanotubes and silver, *Nat. Nano* 5 (2010) 853–857.
- [21] T. Kim, H. Song, J. Ha, S. Kim, D. Kim, S. Chung, J. Lee, Y. Hong, Inkjet-printed stretchable single-walled carbon nanotube electrodes with excellent mechanical properties, *Appl. Phys. Lett.* 104 (2014), 113103.
- [22] S. Park, M. Vosguerichian, Z. Bao, A review of fabrication and applications of carbon nanotube film-based flexible electronics, *Nanoscale* 5 (2013) 1727–1752.
- [23] S. Tuukkanen, M. Hoikkanen, M. Poikelispää, M. Honkanen, T. Vuorinen, M. Kakkonen, J. Vuorinen, D. Lupo, Stretching of solution processed carbon nanotube and graphene nanocomposite films on rubber substrates, *Synth. Met.* 191 (2014) 28–35.
- [24] P.F. Moonen, I. Yakimets, J. Huskens, Fabrication of transistors on flexible substrates: from mass-printing to high-resolution alternative lithography strategies, *Adv. Mater.* 24 (41) (2012) 5526–5541.
- [25] M. Hösel, R.R. Søndergaard, D. Angmo und, F.C. Krebs, Comparison of fast roll-to-roll flexographic, inkjet, flatbed, and rotary screen printing of metal back electrodes for polymer solar cells, *Adv. Eng. Mater.* 15 (10) (2013) 995–1001.
- [26] F.C. Krebs, Fabrication and processing of polymer solar cells: a review of printing and coating techniques, *Sol. Energy Mater. Sol. Cells* 93 (4) (2009) 394–412.
- [27] D. Tobjörk und, R. Österbacka, Paper electronics, *Adv. Mater* 23 (2011) 1935–1961.
- [28] D. Alejandro, A. Escárpita, C. Cárdenas, H. Elizalde, R. Ramirez, O. Probst, Biaxial tensile strength characterization of textile composite materials, *Compos. Prop.* (2012) 83–106, Rijeka, InTech.
- [29] J. Noh, D. Yeom, C. Lim, H. Cha, J. Han, J. Kim, Y. Park, V. Subraman, G. Cho, Scalability of roll-to-roll gravure-printed electrodes on plastic foils, *IEEE Trans. Electron. Packag. Manuf.* 33 (4) (2010) 275–283.
- [30] E. Kipphan, *Handbook of Print Media: Technologies and Production Methods*, Springer-Verlag, Berlin Heidelberg, 2001, pp. 1207.
- [31] M.M. Voigt, R.C. Mackenzie, S.P. King, C.P. Yau, P. Atienza, J. Dane, P.E. Keivanidis, I. Zadrzil, D.D. Bradley und, J. Nelson, Gravure printing inverted organic solar cells: the influence of ink properties on film quality and device performance, *Sol. Energy Mater. Sol. Cells* 105 (2012) 77–85.
- [32] N. Bornemann, H.M. Sauer, E. Dörsam, Gravure printed ultrathin layers of small-molecule semiconductors on glass, *J. Imaging Sci. Technol.* 55 (4) (2011) 40201–40208.
- [33] S.G. Higgins, F.L. Boughey, R. Hills, J.H. Steinke, B.V. Muir, A.J. Campbell, Quantitative analysis and optimization of gravure printed metal ink, dielectric, and organic semiconductor films, *Appl. Mater. Interfaces* 7 (2015) 5045–5050.
- [34] G. Hernandez-Sosa, N. Bornemann, I. Ringle, M. Agari, E. Dörsam, N. Mechau, U. Lemmer, Rheological and drying considerations for uniformly gravure-printed layers: towards large-area flexible organic light-emitting diodes, *Adv. Funct. Mater.* 23 (2013) 3164–3171.
- [35] S. Shian, R.M. Diebold, D.R. Clarke, Tunable lenses using transparent dielectric elastomer actuators, *Opt. Express* 21 (2013) 8669–8676.

- [36] S. De, J.N. Coleman, The effects of percolation in nanostructured transparent conductors, *MRS Bull.* 36 (10) (2011) 774–781.
- [37] K.L. Mills, X. Zhu, S. Takayama, M.D. Thouless, The mechanical properties of a surface-modified layer on polydimethylsiloxane, *J. Mater. Res.* 23 (1) (2008) 37–48.
- [38] C.-Y. Li, Y.-C. Liao, Adhesive stretchable printed conductive thin film patterns on PDMS surface with an atmospheric plasma treatment, *Appl. Mater. Interfaces* 8 (2016) 11868–11874.
- [39] T. Ohishi, H. Noda, T.S. Matsui, H. Jile, S. Deguchi, Tensile strength of oxygen plasma-created surface layer of PDMS, *J. Micromech. Microeng.* 27 (2017) 015015.
- [40] D. Lipomi, M. Vosgueritchian, B. Tee, S.L. Hellstrom, J. Lee, C. Fox, Z. Bao, Skin-like pressure and strain sensors based on transparent elastic films of carbon nanotubes, *Nat. Nanotechnol.* 6 (2011) 788–792.
- [41] B. Sarkar, D.K. Satapathy, M. Jaiswal, Wrinkle and crack-dependent charge transport in a uniaxially strained conducting polymer film on a flexible substrate, *Soft Matter* 13 (32) (2017) 13–32.
- [42] F.A. Bayley, J.L. Liao, P.N. Stavrinou, J.T. Cabral, Wavefront kinetics of plasma oxidation of polydimethylsiloxane: limits for sub-um wrinkling, *Soft Matter* 10 (8) (2014) 1155–1166.

## Biographies



**Iurii Burda** (1991) got his master's degree in Mechanical Engineering from Ivano-Frankivsk National Technical University of Oil and Gas, Ukraine. Since 2014 he works as scientist at the Laboratory for Mechanical Systems Engineering at Empa (Dübendorf, Switzerland). His research activities include fatigue properties of materials, and manufacturing and electro-mechanical characterization of dielectric elastomer actuators.



**Curdin Baechler** (1986) got his master degree in Material Science at the Swiss Federal Institute of Technology Zürich (ETH Zürich) in 2013. Since completing his studies, he is working as a material scientist at the Swiss Laboratory for Material Science and Technology in Dübendorf. He is currently working in the area of printed electrodes for dielectric elastomer actuators.



**Samuele Gardin** (1979) obtained his PhD in Materials Science and Engineering from the University of Padova (Italy) in 2008 under supervision of Prof. Renato Bozio. His focus area has been nonlinear optics, with the design, realization and characterization of solid state distributed feedback laser devices for up-converted lasing. He is currently working as a Scientist at Empa, the Swiss Federal Laboratories for Materials Science and Technology. His competencies include conductive ink preparation, printing-coating-processing and testing of actuator devices.



**Anand Verma** was born in 1985 in Patna, India. He has an engineering degree in Print & Media technology from MIT, Manipal, India and a MSc. degree from TU Chemnitz, Germany with focus on printed electronics. He has diverse printing experiences from conventional printing, digital printing and currently his research is focused on organic & printed electronics. He has gained experiences in printing OLEDs with his work with Novaled GmbH, Dresden, Germany, Holst Center, Eindhoven, The Netherlands and Cynora GmbH, Germany. Since 2015, he is working at Empa as a Coating/printing scientist in functional Polymers group with focus to develop inks & processes for fully printed/coated large area perovskite solar cells. His research area also involves ink development & printing flexible OLEDs, metal oxide inks, batteries, and printed electrodes.



**Giovanni Terrasi** was educated as a material science engineer and received his PhD (Civil Engineering Department) from ETH Zürich in 1997. Between 1998 and 2005 he led the R&D/Engineering Department at SACAC Ltd in Lenzburg, Switzerland with a particular interest in the behavior of high performance concrete reinforced or prestressed with fibre reinforced polymer tendons. Since December 2005 he has been in charge of the Laboratory for Mechanical Systems Engineering at the Swiss Federal Laboratories for Materials Testing and Research, Empa. He has focused his research activities on the in-service durability of mechanical components, on polymer matrix composites, active structures (based on DE actuators and piezoelectric sensors for SHM) and biomechanical engineering.



**Gabor Kovacs** was born in 1958 in Maennedorf, Switzerland. He studied Mechanical Engineering at ETH Zurich and received his Dr. sc. techn. degree at the ETH. Following his PhD he worked at the Institute of Lightweight Structures and Ropeway Technology at the ETH Zurich as senior scientist. From 1996–2001 he was the Head of the competence centre “Aerial Cableway Technology” at Empa in Dübendorf (Zurich). Between 2001 and 2003 he was group leader of electroactive polymers (EAP) actuator technology for adaptive material systems. Between January 2003 and the end of 2005 he was Head of the laboratory for “Materials and Engineering” at Empa. Since 2006 he has been senior scientist for novel actuator technologies in the field of artificial muscles based on EAP. He is the CEO of CTSystems, a spin-off company of EMPA, the ever-first and only manufacturer of commercial dielectric elastomers stack transducers.